Supporting information

Improved H_2O_2 photogeneration and stability on rational tailored polymeric carbon nitride via enhanced O_2 adsorption

Zehao Li *[a, †], Tianxiang Chen [b, †], Yufei Chen [a], Xiaoyuan Chen [a], Le Li [a], Siya Kuang [a], Jing Gao [a], Yuxuan Guo [a], Tsz Woon Benedict Lo [b], Jimin Du *[a]

[a] School of Chemistry and Chemical Engineering, Anyang Normal University, Anyang 455000, China.

[b] State Key Laboratory of Chemical Biology and Drug Discovery, Department of Applied Biology and Chemical Technology, The Hong Kong Polytechnic University, Hunghom, Hong Kong, China

Experimental Section

Characterization

To analyze PCN structure, X-ray diffraction (XRD, Rigaku Corporation Ultima III), Fourier transform infrared spectroscopy (FT-IR, Thermo Scientific Nicolet iS50ATR), X-ray photoelectron spectroscopy (XPS, Thermo Scientific K-Alpha^{+}), and solid-state ^{13}C nuclear magnetic resonance spectroscopy (NMR, Bruker Advance III 500 spectrometer) were performed. The morphology and specific surface area of the obtained PCN were characterized via scanning electron microscopy (SEM, Hitachi SU8010), transmission electron microscopes (TEM, FEI Talos F200X G2), and Brunauer–Emmett–Teller (BET) (Micrometrics Gemini VII 2390) analyses. The optical absorption properties and charge recombination of the obtained PCN were measured via ultraviolet–visible (UV–Vis, Shimadzu UV-2550 UV–vis spectrophotometer) and photoluminescence (PL, Edinburgh FLS980 spectrometer) spectroscopies (under excitation at 370 nm), respectively. The carrier lifetimes were determined at room temperature employing time-resolved PL (Edinburgh FLS980 spectrometer). The adsorptions of NH_3 and O_2 on catalysts were measured via temperature-programmed desorption (TPD) using a chemisorption analyzer (Chembet TPR/TPD Micromeritics 2920). The samples' electron paramagnetic resonance signal was tested using Bruker EMXplus-6/1 (at room temperature with dark and visible light).

Photoelectrochemical measurement

The measurement of the rotating ring-disk electrode (RRDE, Pine Co. Ltd) was

conducted employing a three-electrode cell on a CHI 660E system. Ag/AgCl electrode was used as a reference electrode and carbon rod as a counter electrode. The ring potential of the ring-disk electrode was sustained at 1.40 V (*vs.* RHE). The linear sweep-voltammetry curves were acquired in an O_2-saturated 0.10-M phosphate buffer solution (pH = 6.9) with 5 mV/s. The number of transferred electrons (n) and H_2O_2 production selectivity (s) were calculated using the following equation:

$$n = 4 \times \frac{I_d}{I_d + {I_r}/{N}},$$

$$s = 2 \times \frac{{I_r}/{N}}{\left(I_d + {I_r}/{N}\right)} \times 100\% ,$$

where I_d and I_r are disk and ring current, respectively. The collection efficiency (N) is determined to be 37%.

Electrochemical impedance spectroscopy (EIS), periodic on/off photocurrent response, and Mott–Schottky plots were tested on an electrochemical workstation (Chenhua CHI 660E, Shanghai) employing a conventional three-electrode system.

Photocatalytic H_2O_2 production

First, the photocatalytic H_2O_2-production properties of the obtained samples were screened on a multipass light catalytic reaction system (Perfectlight PCX50C Discover, Beijing) under white LED irradiation. A mass of 0.01-g photocatalyst was adequately dispersed in 50-mL ethanol solution (10 vol%), after which the solution was irradiated under white LED light (30.69 mW/cm^2). The photocatalytic reaction was performed for 1 h at a 15-min interval for sample collection. The H_2O_2

concentration was determined with the colorimetric method, which is based on the peroxidase (POD)-catalyzed oxidation of N, N-diethyl-*p*-phenylenediamine (DPD) using H_2O_2 [1]. Namely, Briefly, 0.1 g of DPD was dissolved in 10 mL 0.05 M H_2SO_4, denoted as solution A. 10 mg of POD was dissolved in 10 mL water, denoted as solution B. 10 mL of 0.1 M Na_2HPO_4 solution and 90 mL of 0.1 M NaH_2PO_4 solution were mixed together to obtain solution C. 1 mL of centrifuged reaction solution, 1.25 mL of distilled water, 0.8 mL of solution C, 50 μL solution A and solution B are mixed. The timedependent H_2O_2 generation was measured as follows: 1 mL filtration from reaction solution was dispersed into solution D, which was monitored by the absorption of the solution at 551 nm and determined with UV–vis spectrophotometer. The calibration curve is prepared with a series of H_2O_2 solutions with known concentrations.

Furthermore, the effects of different alcohols and biomasses on photocatalytic H_2O_2 production employing CNR-0.5 were measured under white LED light irradiation. A mass of 0.01 g CNR-0.5 was dispersed in 50 mL of different aqueous solutions, including methanol (10 vol%), ethanol (10 vol%), isopropanol (10 vol%), glycerol (10 vol%), cyclohexanol (10 vol%), glucose (0.1 g), lactose (0.1 g), and D-cellobiose (0.1 g). The photocatalytic reaction was performed for 1 h at a 15-min interval for sample collection. The H_2O_2 concentration was subsequently measured using the colorimetric method.

To further analyze the performance of samples, the photocatalytic H_2O_2 production employing CNR-0.5 was measured and compared with that of CN using a

300-W Xe lamp comprising a 420-nm UV filter. The average light intensity was 100 mW/cm^2. Mass of 0.04 g of each sample was dispersed in 200-mL aqueous ethanol (10 vol%). The photocatalytic process was performed for 12 h at an interval of 1 h for sample collection. The H_2O_2 concentration was subsequently measured using the colorimetric method.

In order to explore the influence of oxygen on the H_2O_2 generation activity, a mass of 0.01-g photocatalyst was adequately dispersed in 50-mL ethanol solution (10 vol%) or pure water. After that, O_2 was continuously injected into the solution for 10 min under dark conditions to make the O_2 saturated. After 10 min, the flow rate of O_2 was controlled to 300 mL/min. And then the solution was irradiated under white LED light (30.69 mW/cm^2). The photocatalytic reaction was performed for 1 h at a 15-min interval for sample collection. The H_2O_2 concentration was determined with the colorimetric method

The apparent quantum efficiency (AQE) of H_2O_2 formed on CNR-0.5 under conditions of pure water and sacrificial agent were tested separately. The AQE test used a LED light with different wavelengths of 385 nm, 420 nm, 450 nm, 485 nm, and 520 nm (FWHM=15 nm). The AQE was calculated by the following formula:

$$AQE = \frac{2 \times H_2O_2\ formed\ (mol)}{the\ number\ of\ incident\ photons\ (mol)} \times 100\%$$

The solar-to-chemical conversion efficiency test was carried out with CNR-0.5 in pure water and sacrificial agent under LED white light. The solar-to-chemical conversion (SCC) efficiency is determined by the following formula:

$$SCC = \frac{\left[\Delta G_{H_2O_2}\right] \times \left[n_{H_2O_2}\right]}{I \times S \times T} \times 100\%$$

Where $\Delta G_{H_2O_2}$, $n_{H_2O_2}$, I, S, and T represent the free energy for H_2O_2 generation (117 KJ/mol), the molar amount of H_2O_2 generated, the energy intensity of LED white light (30.69 mW/cm^2), the irradiated sample area and the irradiation time (s).

Density functional theory calculations

All calculations based on density functional theory (DFT) were performed using the Material Studio program [2, 3]. The exchange–correlation effects were described by the generalized gradient approximation (GGA)[4] combined with the Perdew–Burke–Ernzerhof (PBE)[5]. The interactions between cores and valence electrons were treated with the projector augmented wave (PAW)[6]. During the calculations, the energy cutoff was set to 571.4 eV. Convergence thresholds of 10^{-5} eV and 0.02 eV/Å were employed for energy and force, respectively. A large vacuum space of 15 Å was used to avoid the periodic boundary condition effects.

The adsorption energies ΔE_{ads} were calculated from the following formula:

$$\Delta E_{ads} = E_{substrate-O_2/C_2H_5OH} - E_{substate} - E_{O_2/C_2H_5OH}$$

where $E_{substrate-O_2/C_2H_5OH}$ and $E_{substate}$ are the total energies for substrate-O_2/C_2H_5OH composites and substrate, respectively. E_{O_2/C_2H_5OH} is the energy of the isolated O_2/C_2H_5OH.

Dissolved oxygen (DO)

The dissolved oxygen concentration in the solution was tested by dissolved oxygen meter (Shanghai Yoke Instrument Limited Company, L-512). First, the DO value in the ethanol solution was tested. And then the catalyst was added into the

solution. After stirring for 30 min under dark conditions, the DO in the reaction solution was tested. The white LED light was turned on immediately. The photocatalytic reaction was performed for 1 h at a 15-min interval for the DO testing.

Results Section

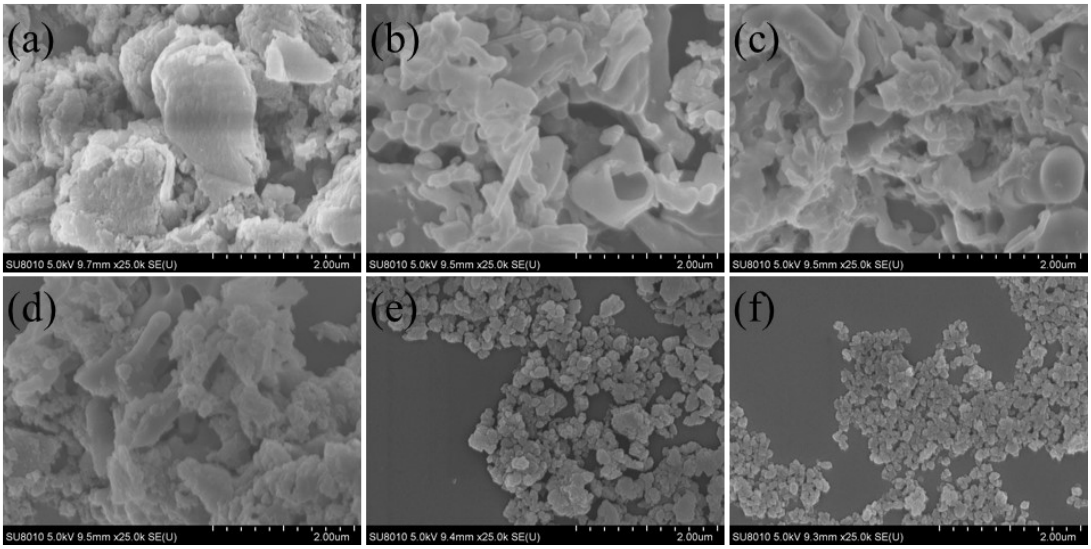

Fig. S1 SEM images of obtained PCN: (a) CN, (b) CN-0, (c) CNR-0.3, (d) CNR-0.5, (e) CNR-0.7, (f) CNR-0.9.

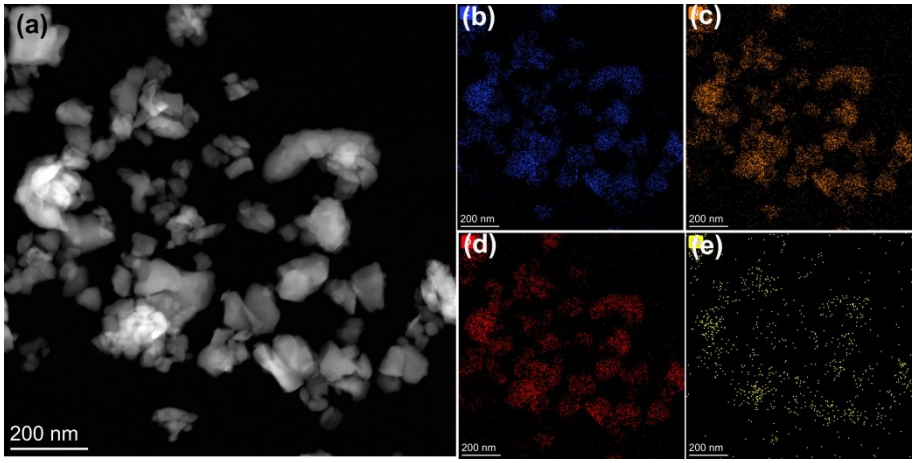

Fig. S2 (a) HAADF-STEM image, (b) C elemental mapping image, (c) N elemental mapping image, (d) O elemental mapping image, (e) Rb elemental mapping image of

CNR-0.5.

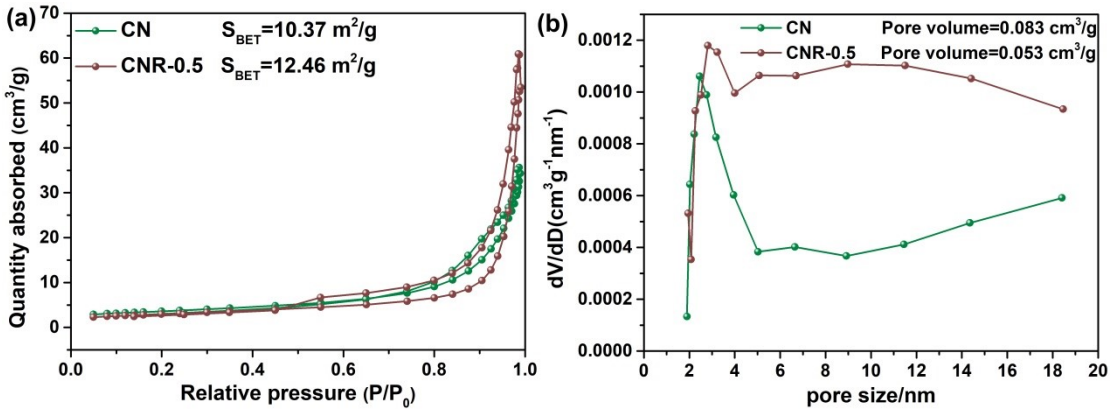

Fig. S3 (a) N_2 adsorption-desorption isotherms. (b) the pore size distribution curves of CN and CNR-0.5.

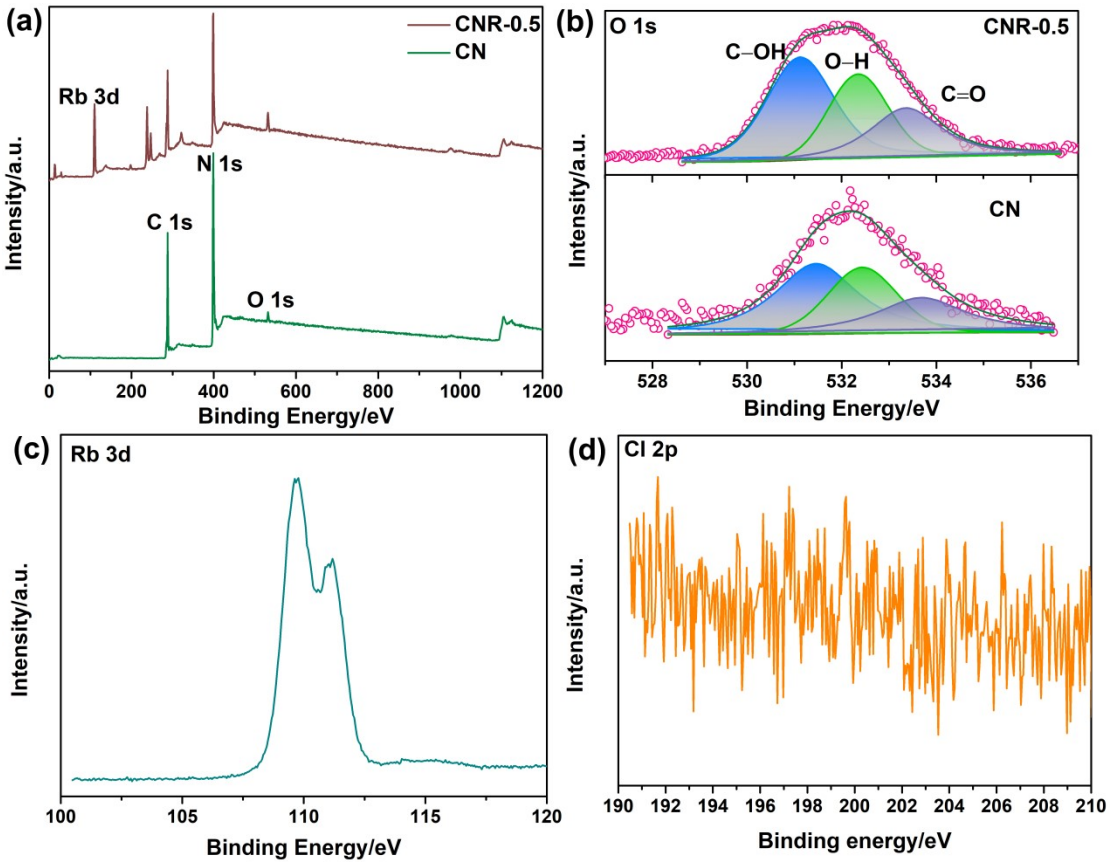

Fig. S4 (a) XPS survey of CN and CNR-0.5. (b) High-resolution XPS spectra of O 1*s* of CN and CNR-0.5. (c) High-resolution XPS spectrum of Rb 3*d* of CNR-0.5. (d)

High-resolution XPS spectrum of Cl 2*p* of CNR-0.5.

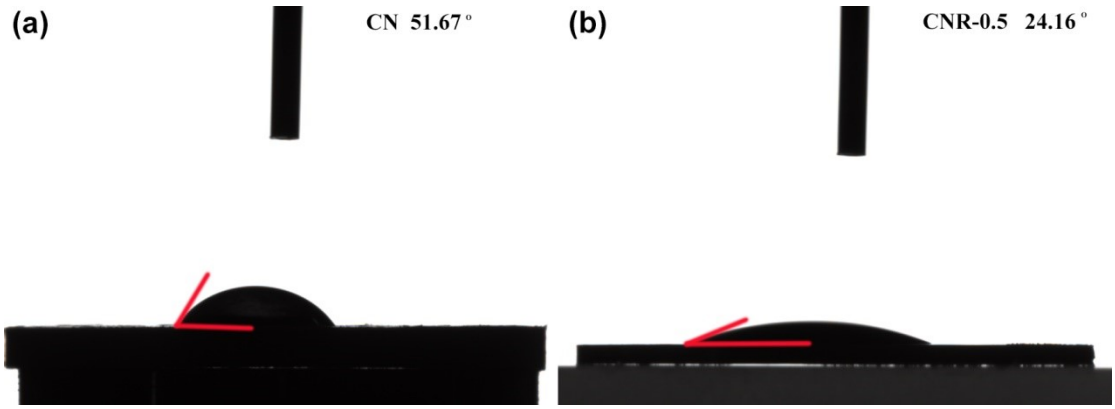

Fig. S5 Digital images of contact angle tests for CN and CNR-0.5.

Fig. S6 The photographs of CN and CNR-0.5 dispersed in deionized water for 7 days.

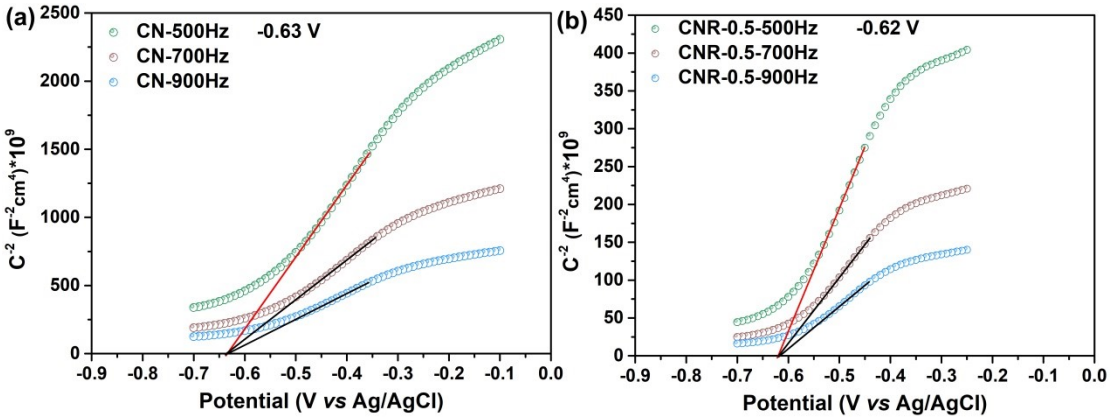

Fig. S7 Mott-Schottky plots in 0.5 M Na_2SO_4 and 0.2 M phosphate buffer electrolyte.

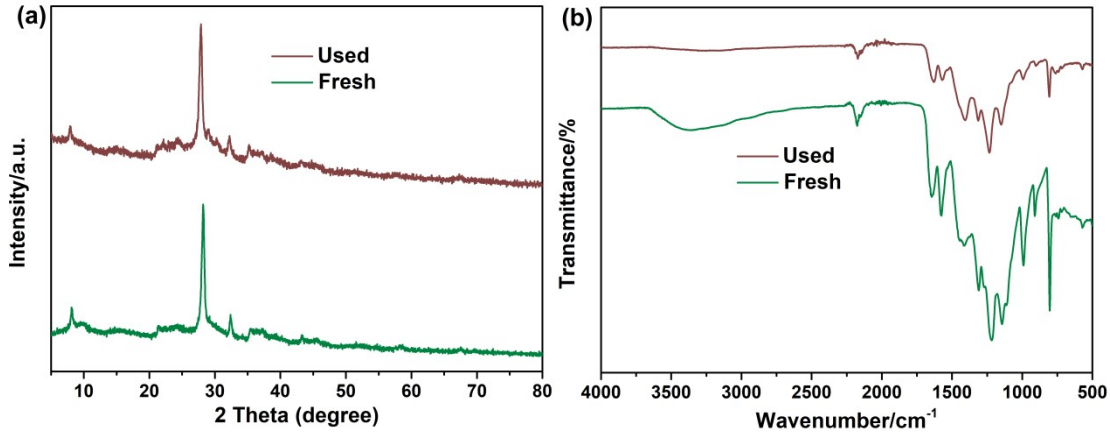

Fig. S8 XRD patterns and FT-IR spectra of the fresh and used CNR-0.5.

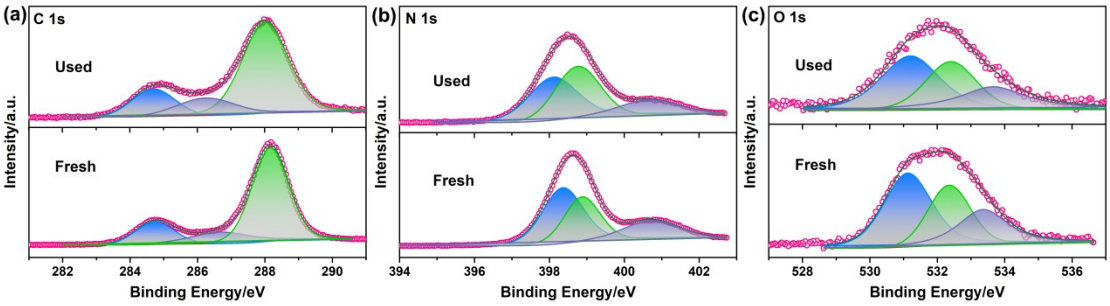

Fig. S9 High-resolution XPS spectra of the fresh and used CNR-0.5.

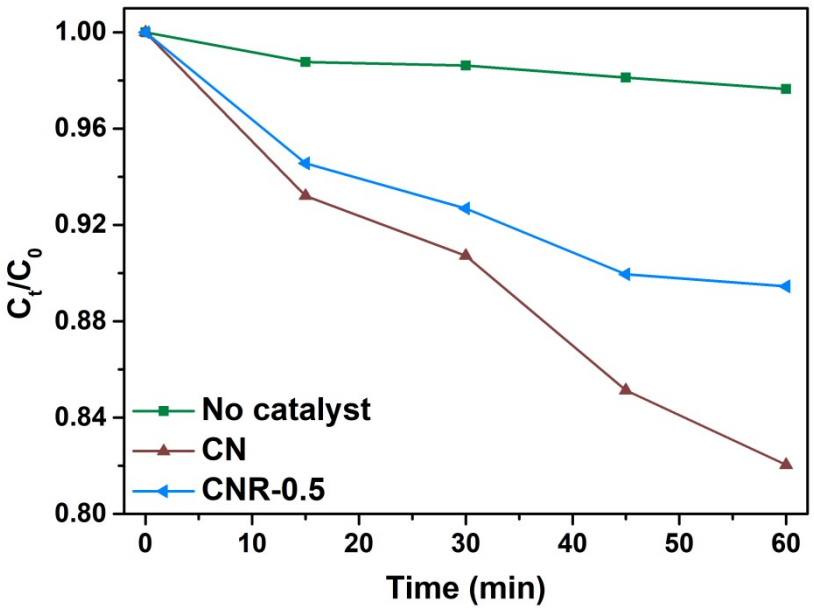

Fig. S10 The photocatalytic decomposition of H_2O_2 for CN and CNR-0.5 under LED white light. The initial concentration of H_2O_2 is 1 mM. And the detailed operation is that 0.01 g of the photocatalyst is adequately dispersed in 50 mL distilled water. After bubbling N_2 for 5 min, turn on LED light. The photocatalytic decomposition is performed for 1 h with a 15-min interval for sample collection. The H_2O_2 concentration was determined by the colorimetric method, which is based on the peroxidase (POD)-catalyzed oxidation of N, N-diethyl-*p*-phenylenediamine (DPD) by hydrogen peroxide.

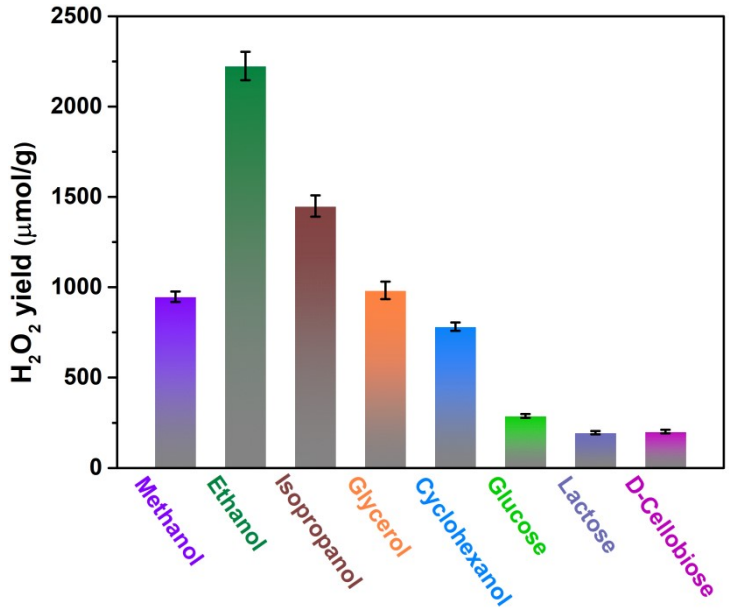

Fig. S11 Photocatalytic H_2O_2 production of CNR-0.5 with different additives under white LED light.

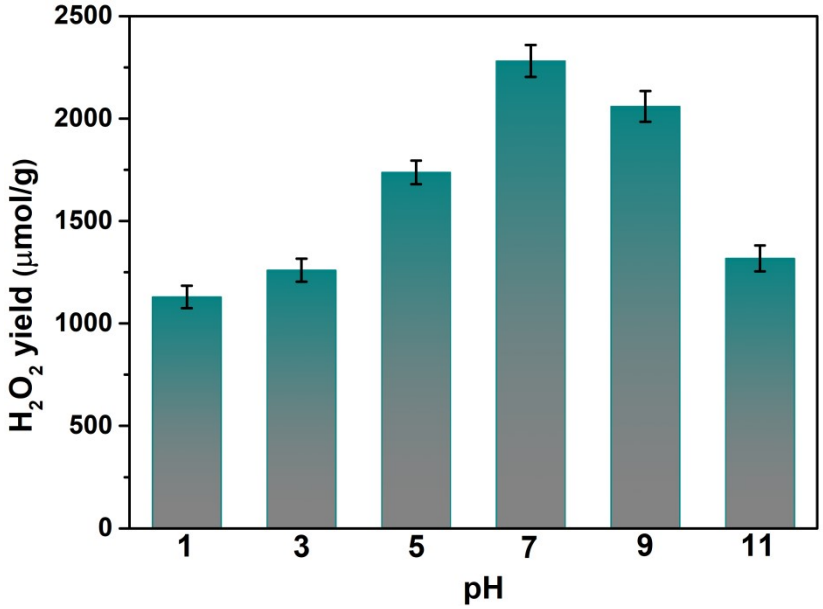

Fig. S12 The photocatalytic H_2O_2 production of CNR-0.5 at different pH values under LED white light irradiation.

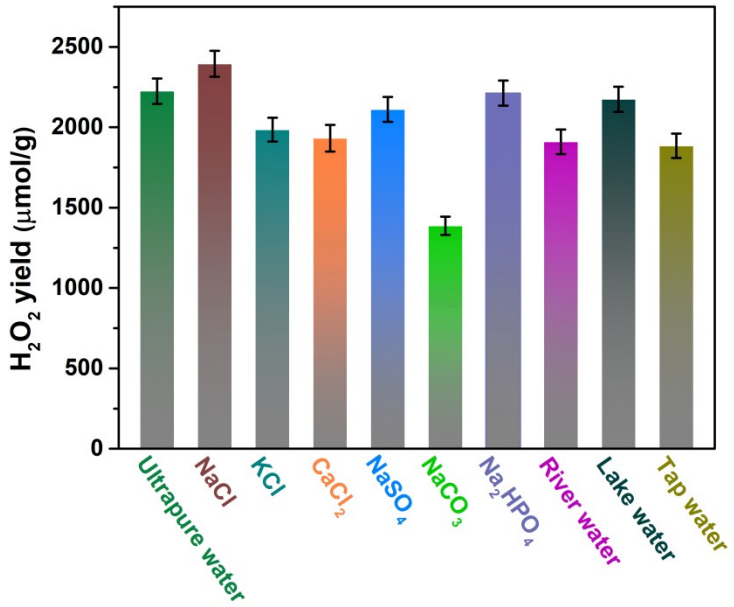

Fig. S13 Effect of different water sources, cations and anions on the photocatalytic H_2O_2 production of CNR-0.5 under LED white light irradiation.

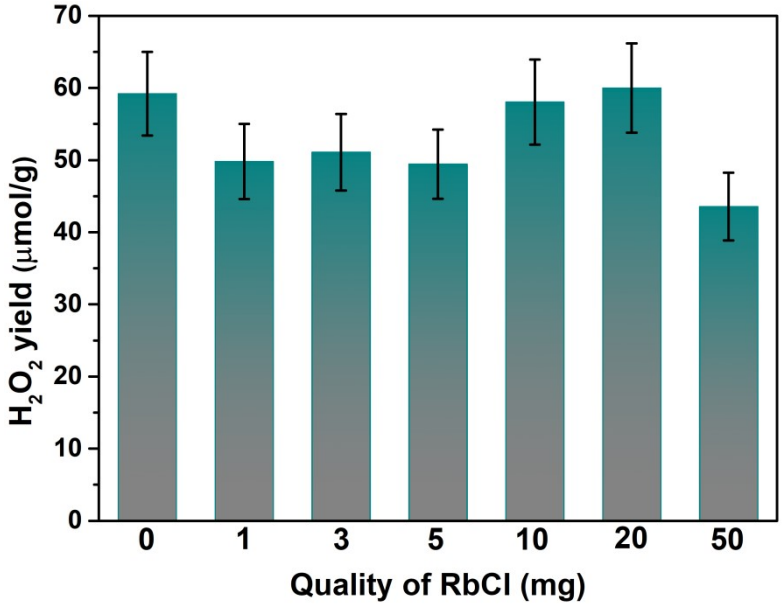

Fig. S14 The photocatalytic H_2O_2 production of CN with RbCl under LED white light irradiation.

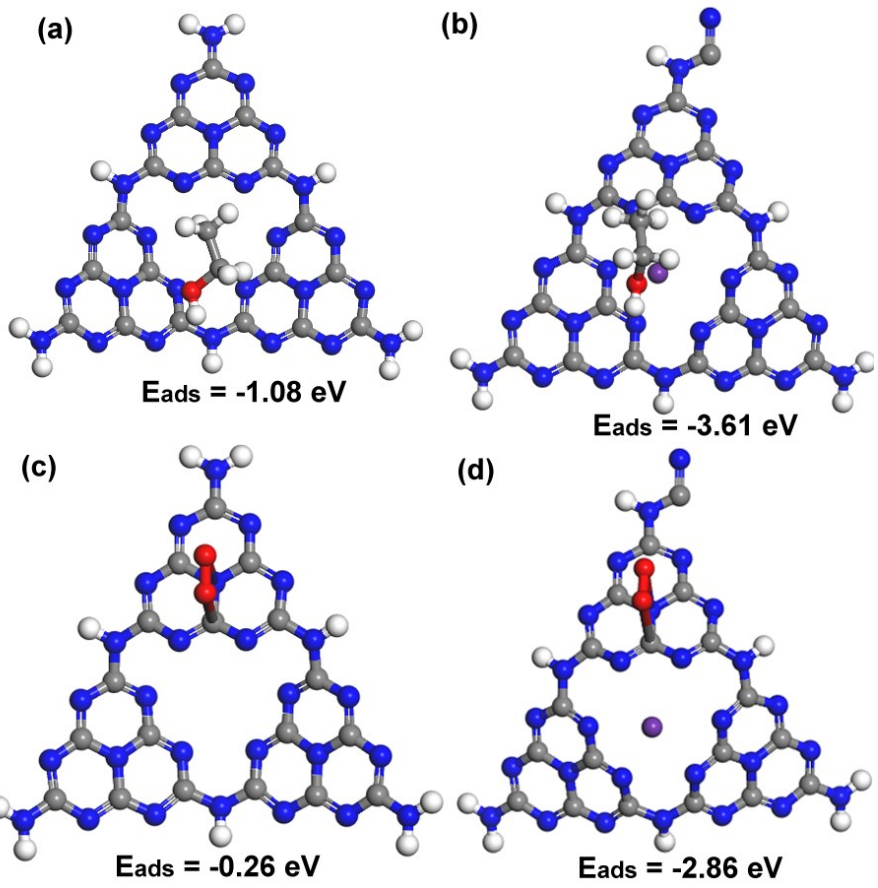

Fig. S15 Top views of optimized geometries for adsorbed molecular ethanol and O_2 on CN and CNR-0.5. (a) CN-ethanol; (b) CNR-0.5-ethanol; (c) CN-O_2; (d) CNR-0.5-O_2.

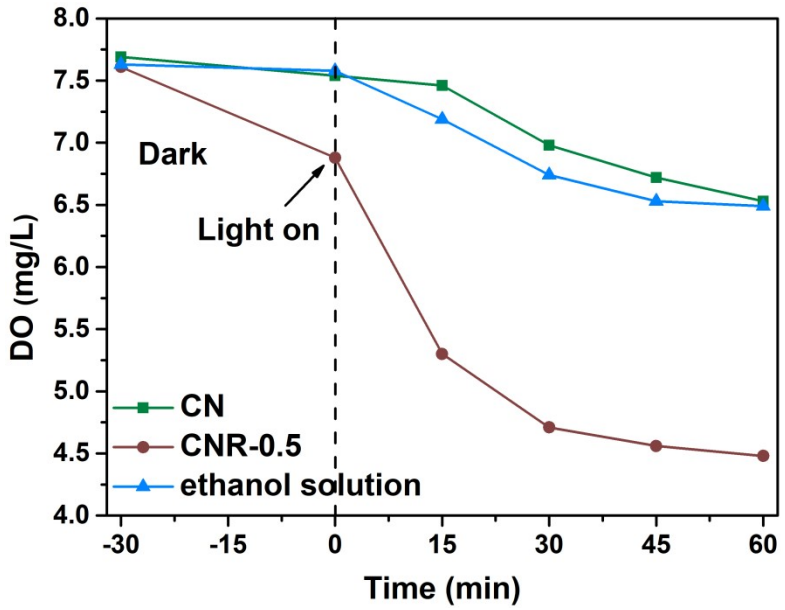

Fig. S16 The dissolved oxygen (DO) concentrations of reaction solution for CN, CNR-0.5, and without catalyst.

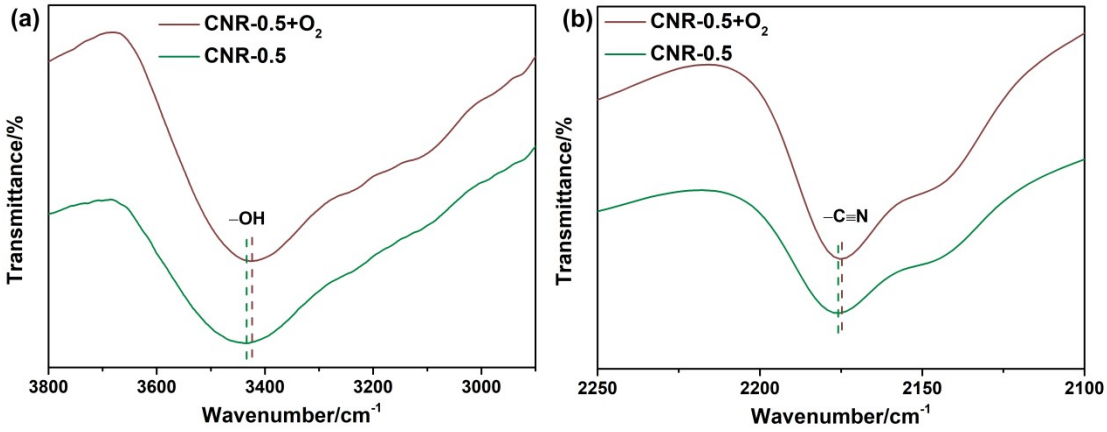

Fig. S17 The FTIR-ATR (attenuated total reflection) spectroscopic study of CNR-0.5 before and after O_2 adsorption. (a) –C≡N group; (b) –OH group. Namely, CNR-0.5 is placed in a vacuum drying oven for dehydration and degassing. Take a part of the sample into a 5 mL centrifuge tube and continuously inject oxygen for 5 min. And then, the FTIR-ATR spectra of them are measured quickly. From the results, after O_2 adsorption, the peaks of –C≡N group and –OH group show a right-shift slightly,

which may be caused by O_2 adsorption of –C≡N/–OH groups.

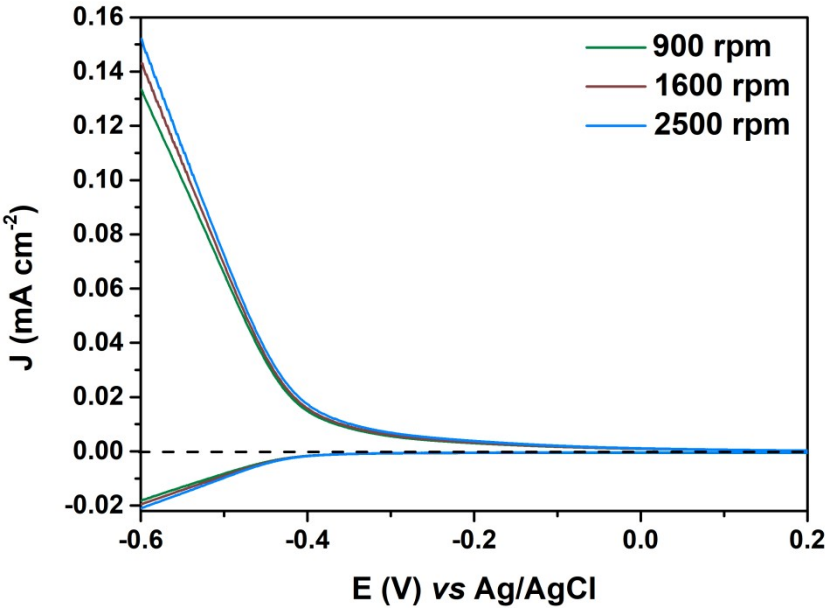

Fig. S18 The RRDE polarization curves of CNR-0.5 at different rotating speeds in O_2-saturated electrolyte along with the ring current and disc current.

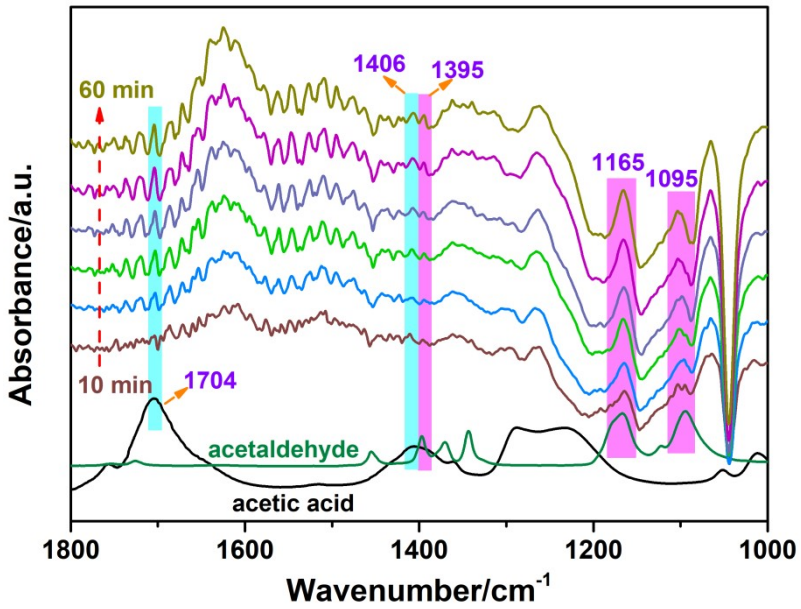

Fig. S19 *In situ* diffuse reflectance infrared Fourier transform spectroscopy of CNR-0.4. The IR spectrum was collected with interval times of 10 min under illumination.

And the spectra of acetic acid and acetaldehyde were obtained by measuring the FT-IR of acetic acid and acetaldehyde, respectively. From the results, we can find that the characteristic peaks of acetaldehyde increase gradually with the reaction time. Furthermore, after 20 min, the characteristic peaks of acetic acid appeared. It can be inferred that ethanol is oxidized to acetaldehyde and a small amount of acetic acid during the reaction.

Table S1. Physicochemical properties of the as-prepared samples.

Sample	S_{BET} (m^2/g)	Pore volume (cm^3/g)
CN	10.37	0.094
CN-0	23.15	0.17
CNR-0.3	6.59	0.037
CNR-0.5	12.46	0.055
CNR-0.7	36.09	0.21
CNR-0.9	58.11	0.27

Table S2 XPS peak area ratio of the as-prepared samples.

Sample	N 1s			Rb (%)[1]	Cl (%)	Rb (%)[2]
	C-N=C	$N-(C)_3$	C-N-H			
CN	49.39%	33.94%	16.67%	-	-	
CNR-0.5	48.31%	32.88%	18.81%	2.06	trace	21.27

Rb (%)[1] means mole percentage from XPS, Rb (%)[2] is mass percentage from inductively coupled plasma (ICP).

Table S3. The adsorption energies of PCN with O_2 and ethanol.

Adsorption	E_{ads} (eV)
$CN + O_2 = CN\text{-}O_2$	-0.26
$CN + CH_3CH_2OH = CN\text{-}CH_3CH_2OH$	-1.08
$CNR + O_2 = CNR\text{-}O_2$	-2.86
$CNR + CH_3CH_2OH = CNR\text{-}CH_3CH_2OH$	-3.61

Table S4. Comparison of the photocatalytic activity of the as-prepared CNR-0.5 with other reported PCN-based photocatalysts.

Samples	Light	Sacrificial agent	ORR (μmol h^{-1} g^{-1})	AQE %	Ref.
Nv-C≡N-CN	400	IPA 10% pH=3	-	36.2	7
PCN-NaCA-2	380	IPA 10%	-	27.6	8
PCN-NaCA-2	420	IPA 10%	-	11.8	8
ORP/GCN	λ>420	Pure water	~165	-	9
AQ/U-POCN	400-780	Pure water	150	-	10
g-C_3N_4/500-85	λ>420	Pure water	~90	-	11
CNOP	λ>420	Pure water	~66.67	-	12
CNOP	420	Pure water	-	2.5	12
KNiCN	λ>420	Pure water	398	-	13
CNR-0.5	420	Ethanol 10%	5802	13.25	This work
CNR-0.5	385	Ethanol 10%	8295	24.52	This work
CNR-0.5	LED white light 20.46 mW/cm^2	Pure water	329.90	-	This work

REFERENCES

1. L. Shi, L. Yang, W. Zhou, Y. Liu, L. Yin, X. Hai, H. Song and J. Ye, *Small*, 2018, **14,** 1703142-1703150.

2. G. Kresse and J. Furthmüller, *Comp. Mater. Sci.*, 1996, **6**, 15-50.

3. G. Kresse and J. Furthmüller, *Phys. Rev. B*, 1996, **54**, 11169-11186.

4. J. P. Perdew, K. Burke and M. Ernzerhof, *Phys. Rev. Lett.*, 1996, **77**, 3865-3868.

5. J. P. Perdew, M. Ernzerhof and K. Burke, *J. Chem. Phys.*, 1996, **105**, 9982-9985.

6. G. Kresse and D. Joubert, *Rev. B*, 1999, **59**, 1758-1775.

7. X. Zhang, P. Ma, C. Wang, L. Gan, X. Chen, P. Zhang, Y. Wang, H. Li, L. Wang, X. Zhou and K. Zheng, *Energ. Environ. Sci.*,, 2022, **15**, 830-842.

8. Y. Zhao, P. Zhang, Z. Yang, L. Li, J. Gao, S. Chen, T. Xie, C. Diao, S. Xi, B. Xiao, C. Hu and W. Choi, *Nat. Commun.*, 2021, **12**, 3701-3711.

9. J. Zhang, J. Lang, Y. Wei, Q. Zheng, L. Liu, Y.-H. Hu, B. Zhou, C. Yuan and M. Long, *Appl. Catal. B: Environ.*, 2021, **298**, 120522.

10. Y.-X. Ye, C. Wen, J. Pan, J.-W. Wang, Y.-J. Tong, S. Wei, Z. Ke, L. Jiang, F. Zhu, N. Zhou, M. Zhou, J. Xu and G. Ouyang, *Appl. Catal. B: Environ.*, 2021, **285**, 119726.

11. B. Liu, J. Du, G. Ke, B. Jia, Y. Huang, H. He, Y. Zhou and Z. Zou, *Adv. Funct. Mater.*, 2021, DOI: 10.1002/adfm.202111125, 2111125-2111136.

12. H. Kim, K. Shim, K. E. Lee, J. W. Han, Y. Zhu and W. Choi, *Appl. Catal. B: Environ.*, 2021, DOI: 10.1016/j.apcatb.2021.120666, 120666.

13. Y. Chen, X. Yan, J. Xu and L. Wang, *J. Mater. Chem. A*, 2021, **9**, 24056-24063.